JOURNAL OF GEOPHYSICAL RESEARCH: OCEANS, VOL. 118, 1830–1844, doi:10.1002/jgrc.20135, 2013

Assessment of Southern Ocean water mass circulation and characteristics in CMIP5 models: Historical bias and forcing response

J.-B. Sallée,[1] E. Shuckburgh,[1] N. Bruneau,[1] A. J. S. Meijers,[1] T. J. Bracegirdle,[1] Z. Wang,[2] and T. Roy[3]

Received 1 August 2012; revised 4 January 2013; accepted 18 February 2013; published 9 April 2013.

[1] The ability of the models contributing to the fifth Coupled Models Intercomparison Project (CMIP5) to represent the Southern Ocean hydrological properties and its overturning is investigated in a water mass framework. Models have a consistent warm and light bias spread over the entire water column. The greatest bias occurs in the ventilated layers, which are volumetrically dominated by mode and intermediate layers. The ventilated layers have been observed to have a strong fingerprint of climate change and to impact climate by sequestrating a significant amount of heat and carbon dioxide. The mode water layer is poorly represented in the models and both mode and intermediate water have a significant fresh bias. Under increased radiative forcing, models simulate a warming and lightening of the entire water column, which is again greatest in the ventilated layers, highlighting the importance of these layers for propagating the climate signal into the deep ocean. While the intensity of the water mass overturning is relatively consistent between models, when compared to observation-based reconstructions, they exhibit a slightly larger rate of overturning at shallow to intermediate depths, and a slower rate of overturning deeper in the water column. Under increased radiative forcing, atmospheric fluxes increase the rate of simulated upper cell overturning, but this increase is counterbalanced by diapycnal fluxes, including mixed-layer horizontal mixing, and mostly vanishes.

Citation: Sallée, J.-B., E. Shuckburgh, N. Bruneau, A. J. S. Meijers, T. J. Bracegirdle, Z. Wang, and T. Roy (2013), Assessment of Southern Ocean water mass circulation and characteristics in CMIP5 models: Historical bias and forcing response, *J. Geophys. Res. Oceans*, *118*, 1830–1844, doi:10.1002/jgrc.20135.

1. Introduction

[2] The Southern Ocean is the dominant anthropogenic carbon sink of the world's oceans and plays a central role in the redistribution of physical and biogeochemical properties around the globe [*Sarmiento et al.*, 2004]. Recent Southern Ocean studies have suggested a slowdown of the carbon sequestration, an overall warming and decrease of the rate of ventilation of the intermediate water masses, as well as some hints of a desalinization in the vicinity of Antarctica [*Le Quéré et al.*, 2007; *Gille*, 2002; *Rintoul*, 2007]. These changes are fundamental to the global climate and are directly associated with the meridional overturning of water masses. Therefore, one of the most pressing issues in oceanography is to understand the rate, the structure and the controls of the water mass overturning circulation in the Southern Ocean and to accurately represent these aspects in climate models.

[3] Most of the world's oceanic water masses are either formed or modified within the Southern Ocean overturning circulation [*Sverdrup et al.*, 1942; *Marshall and Speer*, 2012]. As shown schematically in Figure 1, the zonal-mean Southern Ocean overturning water mass circulation is thought to involve an upper and lower branch. Circumpolar Deep Water (CDW) formed in the North Atlantic enters the Southern Ocean and is largely uplifted to feed both the upper and the lower branches. In the upper branch, CDW is converted in northward flowing Mode Waters (MW) and Intermediate Waters (IW). In the lower branch, Circumpolar Deep Water is converted into northward flowing bottom waters [e.g., *Sloyan and Rintoul* 2001].

[4] The two-cell structure of the Southern Ocean water mass overturning circulation was first revealed by the meridional hydrographic structure of the Southern Ocean [e.g., *Deacon*, 1937; *Sverdrup et al.*, 1942]. However, because of the absence of zonal barriers and the associated importance of the eddy-induced flow in the meridional circulation, assessing and monitoring the intensity of the overturning circulation has always been challenging. Two approaches have been explored in the past to infer the circulation from observations: either from water mass formation and trans-

[1]British Antarctic Survey, Cambridge, UK.
[2]School of Marine Sciences, Nanjing University of Information Science and Technology, Nanjing, China.
[3]Laboratoire d'océanographie et du climat: expérimentations et approches numériques, Paris, France.

Corresponding author: J.-B. Sallée, British Antarctic Survey, High Cross, Madingley Road, Cambridge CB30ET, UK. (jbsallee@gmail.com)

2169-9275/13/10.1002/jgrc.20135

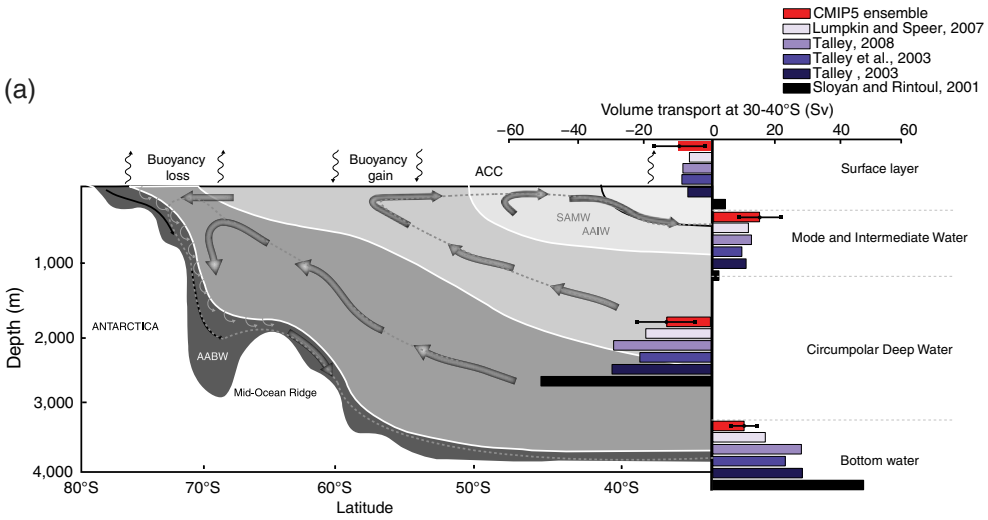

Figure 1. Southern Ocean Water masses circulation. Schematic of the two cell meridional overturning circulation in the Southern Ocean (adapted from *Speer et al*., 2000 and *Meredith et al*., 2011). Five observation-based estimates of the volume transports in different water mass classes at 30°–40°S are superimposed along with corresponding estimate from the CMIP5 model ensemble. The five observation-based estimates are shown in purple/black bars, while the red bars show the multi-model CMIP5 ensemble. The multi-model spread around the mean is shown by the black lines superimposed on top of the red bars and represent the multi-model standard deviation.

formation at the ocean surface [e.g., *Speer et al.*, 2000; *Sallée et al.*, 2006; *Sallée et al.*, 2010], or from water mass transport in and out of the Southern Ocean across the 30°S boundary [*Sloyan and Rintoul*, 2001; *Talley*, 2003; *Talley et al.*, 2003; 2008; *Lumpkin and Speer*, 2007]. The results of the second approach are indicated in Figure 1 (blue bars). However, despite many attempts to estimate the overturning intensity, significant uncertainty still remains as to the magnitude of and the processes responsible for this circulation.

[5] The structure of the water mass conversion in general circulation models can differ significantly from one model to another and from that suggested by observation-based estimates [*Gnanadesikan et al.* 2004; *Downes et al.* 2009; 2010; 2011]. Given the importance of the Southern Ocean water masses for global climate, the lack of understanding and consistency in modeling the Southern Ocean water mass conversion represents a significant challenge for the climate science community; particularly with regard to providing robust projections of future climate change. For instance, it remains unclear whether the inconsistency between model simulations arises from differences in atmospheric fluxes, ocean model physics, or the way in which the flow is broken down into water mass classes. The goal of this study is to shed further light on these issues by consistently assessing water mass hydrological characteristics (i.e., temperature, salinity and density, hereafter referred to as water mass characteristics), as well as water mass formation and transport in a range of climate models run for the fifth Coupled Model Intercomparison Project (CMIP5). In particular, we investigate projected changes under future radiative forcing scenarios. Here, we present an assessment of the historical state and projected changes of the Southern Ocean circulation water mass in 21 CMIP5 models using a water mass framework.

[6] After presenting the model output and the water mass definition procedure, we will focus our analysis on the simulation of the water mass characteristics in historical runs and tackle how they are predicted to change under increased radiative forcing. The simulation of the Southern Ocean water mass overturning will then be investigated before finishing with a discussion of the results.

2. Data and Methods

2.1. CMIP5 Models and Observation-based Products

[7] Outputs from a series of CMIP5 climate models are assessed in this study [*Taylor et al.*, 2012]. The required variables were downloaded from the British Atmospheric Data Centre portal (http://badc.nerc.ac.uk/home/index.html). Variables from both the ocean and atmosphere components of the model were used (temperature, salinity, pressure and velocities for the ocean components; wind stress and heat and freshwater air-sea fluxes for the atmospheric component). Twenty-one models with all the required ocean parameters were used, while only 14 models had both atmospheric and ocean parameters available (see Table 1).

[8] The present day mean state of the models is assessed through comparisons with observation-based estimates of the Southern Ocean water mass structure and circulation. For these comparisons, we used data from "historical" forcing runs, which are fully coupled experiments forced by 20th century variations of important natural and anthropogenic climate drivers. The term "present day" is defined here as the 30 year period 1976–2005.

[9] A combination of ocean parameters has been used to assess the models' present state. Transport at 30°S has been collated from five distinct observation-based studies,

Table 1. Details of Models Used in CMIP5 Analysis of Southern Ocean[a]

Number	Model Name	HIST	RCP45	RCP85	Vertical	Resolution at 50°S
1	bcc-csm1-1	O	O		Z	1.0 × 1.0
2	CanESM2	O		O	Z	1.41 × 0.93
3	CCSM4	O	O		Z	1.13 × 0.53
4	CNRM-CM5	O/A			Z	1.0 × 0.65
5	CSIRO-Mk3-6-0	O/A	O		Z	1.88 × 0.93
6	GFDL-ESM2G	O/A	O/A	O/A	S	1.0 × 1.0
7	GFDL-ESM2M	O/A	O	O/A	Z	1.0 × 1.0
8	GISS-E2-H	O			Z	1.0 × 1.0
9	GISS-E2-R	O/A	O	O	Z	1.25 × 1.0
10	HadCM3	O/A			Z	1.25 × 1.25
11	HadGEM2-CC	O/A	O	O	Z	1.0 × 1.0
12	HadGEM2-ES	O/A	O	O	Z	1.0 × 1.0
13	inmcm4	O	O		S	1.0 × 0.47
14	IPSL-CM5A-LR	O/A	O	O	Z	1.98 × 1.30
15	IPSL-CM5A-MR	O/A	O/A		Z	1.98 × 1.30
16	MIROC5	O/A	O/A		SZ	1.41 × 0.78
17	MIROC-ESM	O/A	O/A	O/A	SZ	1.41 × 0.93
18	MIROC-ESM-CHEM	O/A	O/A		SZ	1.41 × 0.93
19	MPI-ESM-LR	O/A	O/A	O/A	Z	1.41 × 0.89
20	MRI-CGCM3	O	O	O	Z	1.0 × 0.5
21	NorESM1-M	O		O	S	1.13 × 0.53

[a]For each column "O" means that we used the ocean component, and "A" means that we used the atmospheric component. Vertical refers to the vertical coordinate scheme, where Z indicates depth level and S sigma coordinates (SZ are hybrids). Resolution is zonal mean ocean grid longitude and latitude differences at 50°S. ESM (Earth System Model) indicates if model includes a coupled carbon cycle.

all based on repeat hydrographic sections arising from the WOCE and CLIVAR programs [*Sloyan and Rintoul*, 2001; *Talley*, 2003; *Talley et al.*, 2003; 2008; *Lumpkin and Speer*, 2007]. The climatological state of the three-dimensional ocean interior has been estimated from the CARS2009 climatology (http://www.marine.csiro.au/ dunn/cars2009/; *Ridgway et al.*, [2002]).

[10] The future projections of the CMIP5 models are assessed by considering two future scenarios: the Representative Concentration Pathway (RCP) 4.5 and RCP 8.5, where the numbers refer to the approximate radiative forcing change by the year 2100. RCP4.5 is a medium mitigation scenario and RCP8.5 is a high emissions scenario. These scenarios include a full range of anthropogenic forcing factors (GHGs, aerosols, chemically active gases and land use) along with a repeating 11 year solar cycle (repeating solar cycle 23), which are detailed in *Meinshausen et al.* [2011]. All the models include a representation of stratospheric ozone changes [see information about ozone forcing *Bracegirdle et al.*, 2013; we note that not all models use the same ozone forcing, and thus the effect may be of different intensity in the different models]. We consider both atmosphere-ocean general circulation models (AOGCMs) driven by GHG concentration time series and Earth system models (ESMs) driven by GHG emissions time series. In this paper, 21st century change is defined as the difference between the mean over the period 2070–2099 following either RCP8.5 or RCP4.5 minus the mean over the period 1976–2005 in the historical experiment. The "r1i1p1" runs from each scenario were used in this study.

2.2. Definition of the Southern Ocean Water Masses

[11] The challenge in comparing the large-scale structure of several ocean models is to make sure the comparison is done in a consistent framework across the different models. Water masses are tightly linked to the large-scale ocean dynamical processes, and are therefore unequivocal in characterizing the large-scale circulation structures in the ocean [e.g., *Iudicone et al.*, 2010]. In addition, they are also critical to identifying and understanding changes in the circulation pattern and ocean properties [*Bindoff and McDougall*, 2000].

[12] Therefore, the challenge comes down to developing an objective and automatic procedure to identify water masses that can be reliably applied to all models analyzed, both for their historical and future scenario runs. In this paper, we chose to focus on five water masses that are crucial for the Southern Ocean overturning circulation, namely from light to dense: surface subTropical Water (TW), Mode Water (MW), Intermediate Water (IW), Circumpolar Deep Water (CDW) and Antarctic Bottom Water (AABW). These five water masses cover the entire Southern Ocean watercolumn. We define the five water masses by finding their most appropriate potential density envelope (referenced to 2000 m: σ_2). Therefore, the potential density envelope that we use differ from model to model.

[13] Intermediate water is associated with a significant local salinity minimum and, out of the five water masses, has the strongest signal in hydrological properties. We therefore start the procedure of water mass definition by finding the density envelope associated with intermediate water. We then switch to the mode water, which is directly above the intermediate water. Mode water is associated with a minimum in potential vorticity [PV, i.e., weak stratification; *McCartney*, 1977]. We therefore set the upper end of the mode water density envelope by assuming that the mode water density envelope must encompass at least 90% of the local minima in PV. Surface subtropical water is defined as the layer that is lighter than the mode water. Finally, we set the bottom water density envelope to cover the entire very weakly stratified layer lying at the bottom of the ocean. Circumpolar deep water is then defined as the layer between bottom and intermediate water.

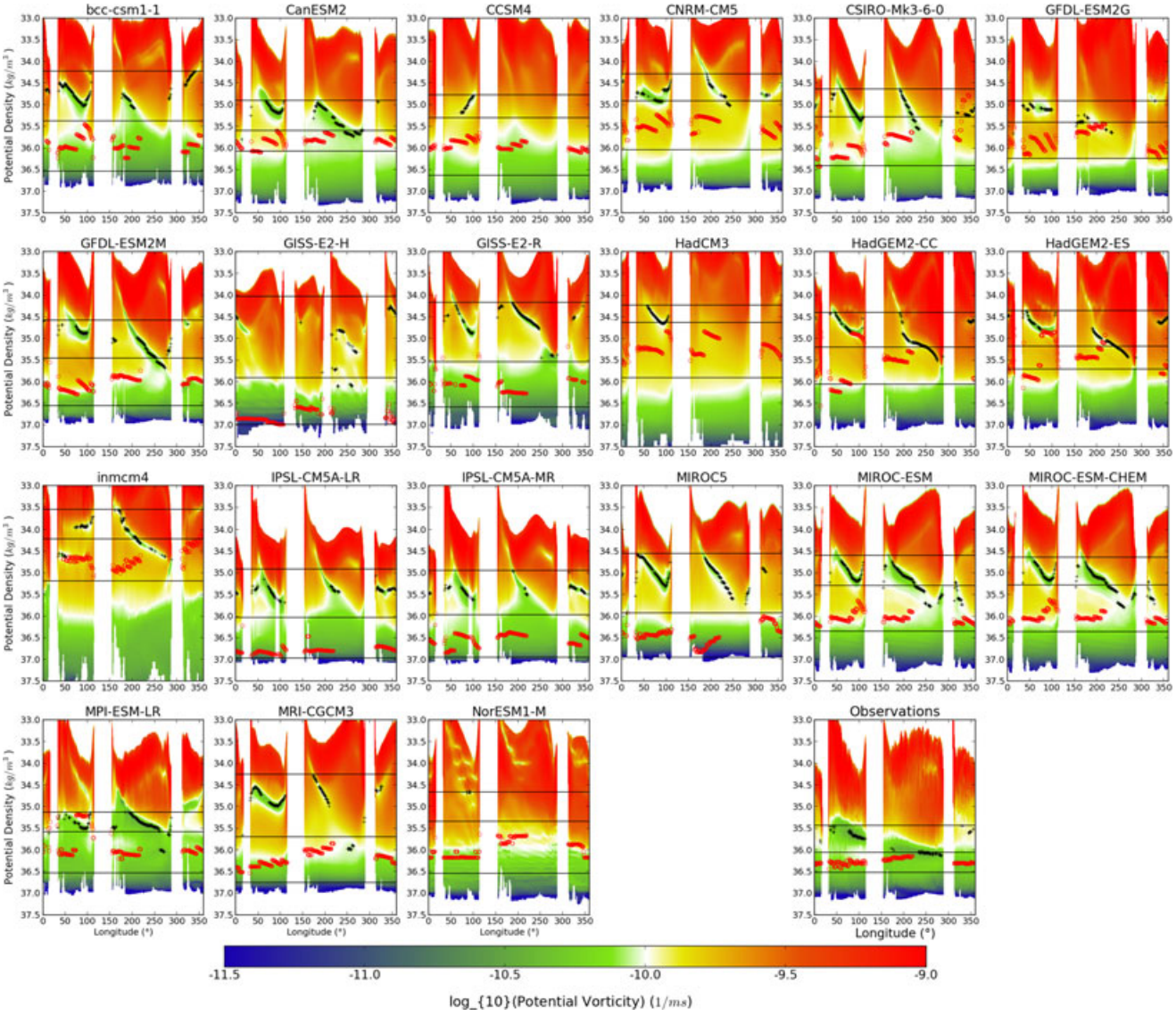

Figure 2. Historical section of potential vorticity at 30°S in density coordinates for the 21 models. Observations (lower right panel) taken from CARS09. Black crosses show the local minimum of potential vorticity ($\log_{10}$ of PV is shown, $m^{-1}\ s^{-1}$) as detected by our definition (see section 2). Red crosses show the locations of the local minimum of salinity. The three horizontal black lines show the potential density of the boundaries between water masses, and in order of lightest to densest, these are: (a) subtropical water/mode water; (b) mode water/intermediate water; (c) intermediate water/circumpolar deep water.

[14] An important feature of our definition is that it does not assume any property range in which a particular water mass should lie. That allows us to apply the definition to very different models, even those that are strongly skewed or those with large offsets in properties. We now detail in turn the choices made for the definition of intermediate water, mode water and bottom water.

[15] As illustrated in *Sallée et al.* [2010], both intermediate and mode water have strong regional variations that can be clearly seen at the northern edge of the Southern Ocean on a meridional circumpolar section (30°S). When identifying the water masses, we therefore use a climatological mean of a 30°S section to define mode and intermediate water. In contrast, we use a climatological zonal mean when defining bottom water, since this is more clearly defined at high latitudes.

[16] At 30°S, at each half degree of longitude around the circumpolar belt, the climatological mean salinity profile is analyzed to find the intermediate water envelope. On the profile, we search for the salinity minimum S_{min} (Figure 2, red crosses), along with the maxima directly above (S_{max_above}) and directly below (S_{max_below}). The upper end of the envelope, $\sigma_2(IW^+)$, is set at a quarter of the distance (in density space) between S_{min} and S_{max_above}: $\sigma_2(IW^+) = (3\sigma_2(S_{min}) + \sigma_2(S_{max\_above}))/4$. Similarly, the lower end of the envelope, $\sigma_2(IW^-)$, is set at a quarter of the distance (in density space) between S_{min} and S_{max_below}: $\sigma_2(IW^-) = (3\sigma_2(S_{min}) + \sigma_2(S_{max\_below}))/4$. This is repeated

for each profile around the circumpolar belt at 30°S and then averaged to find the intermediate water envelope: $\{\overline{\sigma_2(IW^-)}; \overline{\sigma_2(IW^-)}\}$.

[17] At 30°S, at each half degree of longitude around the circumpolar belt, the climatological mean PV profile is also analyzed to find the associated mode water envelope. On the profile, we search for a local minimum in PV, i.e., a minimum that must be bound by maxima above and below. In order to discriminate between a local minimum associated with mode water and other categories of local minimum, we added the requirement that the parcel of water must be weakly stratified [*McCartney*, 1977]. We therefore search for a local minimum associated with stratification weaker than 0.1 kg m^{-3} per 50 m (i.e., PV $\sim 10^{9.7}$ m^{-1} s^{-1}). If a local minimum satisfying these criteria, $PV_{localmin}$, is found, we treat it as a parcel of mode water (Figure 2, black crosses). We repeat this process for all profiles around the circumpolar belt at 30°S, and then set the upper end of the mode water layer, $\sigma_2(MW^+)$, so that the mode water envelope encompasses at least 90% of the sum of $PV_{localmin}$ found around the circumpolar belt (the lower end of the layer is set as the upper end of the intermediate water layer, i.e., $\sigma_2(MW^-) = \sigma_2(IW^+)$).

[18] Finally, we set the upper end density of the bottom water envelope, $\sigma_2(AABW^+)$, so it includes any water for which PV is smaller than five times the minimum of PV found at the bottom of the ocean.

[19] The arbitrary constants used in these definitions (25% for intermediate water, 90% for mode water, and 500% for bottom water) have all been manually adjusted to best capture the five water masses in each model analyzed. The water mass boundaries found by the automatic procedure are superimposed on the 30°S section of PV (Figure 2) and the zonal-mean sections of salinity (Figure 3) for each model.

[20] While the water mass boundaries found by the automatic procedure are very satisfactory, we acknowledge that the classical approach often used for single model analysis, which consists of setting water mass boundaries "by eye", would do a better job in a few instances. However, we note that here our goal is to find a systematic and consistent definition that can be applied equally to all models, so that the comparisons are repeatable and as objective as reasonably possible.

2.3. Water Mass Transformation and Formation

[21] To analyze the impact of surface fluxes on water mass transformation and to separate them from interior processes, we use the same formalism that *Downes et al.* [2011] applied to the ocean reanalysis and the GFDL climate models. The formalism was first proposed by *Walin* [1982] and since then has been applied in numerous studies [e.g., *Tziperman* 1986; *Speer and Tziperman*, 1992; *Marshall et al.* 1999]. Here, we present a brief summary of the terms and notation of *Downes et al.* [2011].

[22] A density layer bounded by the density σ_2^k and σ_2^{k+1} can either inflate or deflate due to water mass formation. We consider two types of water mass formation. First, the water mass formation, ΔF, resulting from ocean-atmosphere or ocean-ice buoyancy flux; Second, the "interior" water mass formation, ΔD, which we define as any other kind of diapycnal fluxes, such as interior diapycnal mixing, diapycnal mixing in the mixed layer, cabbeling, thermobaricity, etc. Because we are analyzing the Southern Ocean basins only, the density layer volume change, and water mass formation can be balanced by the volume transport across the 30° S boundary, $\Delta\Psi_{30S}$:

$$\frac{\mathrm{d}V_k}{\mathrm{d}t} - \Delta\Psi_{30S} = \Delta F + \Delta D, \tag{1}$$

where V_k is the volume of the density layer bounded by the density σ_2^k and σ_2^{k+1}.

[23] The transport at 30°S and the volume change with time are directly computed from the ocean component of the model. The surface formation is derived from the surface transformation across the density σ_2^k, F^k, which results from heat and freshwater buoyancy fluxes:

$$F^k = \frac{1}{\sigma_2^{k+1} - \sigma_2^k} \iint_{\mathcal{A}} \frac{\alpha Qnet}{Cp} d\mathcal{A} + \iint_{\mathcal{A}} \rho_0 \beta S \mathcal{F} \mathrm{d}\mathcal{A}, \tag{2}$$

where $\mathcal{A}$ is the area of the density σ_2^k outcrop, *Qnet* and $\mathcal{F}$ are the heat and freshwater fluxes, and α and β are the thermal and haline contraction coefficients. Because of the large seasonal variability in buoyancy fluxes and in outcrop area, the computation of F^k is performed on monthly climatological mean, before being averaged into annual means.

[24] Once the transport at 30°S, the volume change, and the surface formation have been computed, we infer interior formation using equation (1).

3. Historical Representation of Water Masses in CMIP5 Models

[25] The different climate models analyzed vary widely in their ability to recreate climatological water masses (Figures 2 and 3). In this section, we investigate the ability of the climate models to simulate the most basic properties (temperature, salinity, volume, outcrop area) of each of the water masses.

3.1. Surface Subtropical Water

[26] All models consistently simulate warmer surface subtropical water than those observed (Figure 4a). The warm bias is as large as 4–6°C for *GISS-E2-H* and *incmcm4*. All other models have a bias of 1–3°C, except *MPI-ESM-LR*, *GFDL-ESM2G*, and *CanESM2*, which simulate subtropical water temperature more realistically. The overall warm bias is reflected in the multi-model mean, which has a subtropical water temperature of 16.5°C compared with an observed value of 13.8°C (Table 2). This large and significant surface warm bias is consistent with very large discrepancies that exist between model and observation-based estimates of the cumulative heat flux into the Southern Ocean surface in the last 50 years [Frölicher et al., manuscript in preparation. *Anthropogenic heat and carbon uptake by the Southern Ocean in CMIP5 models*]. In comparison, the multi-model bias in salinity is much smaller (a fresh bias of 0.19 psu, Table 2). The density of subtropical waters is strongly affected by the offset in temperature. For instance, subtropical water in *incmcm4* is lighter than that observed by more than 2 kg m^{-3} (Figure 4a). In addition

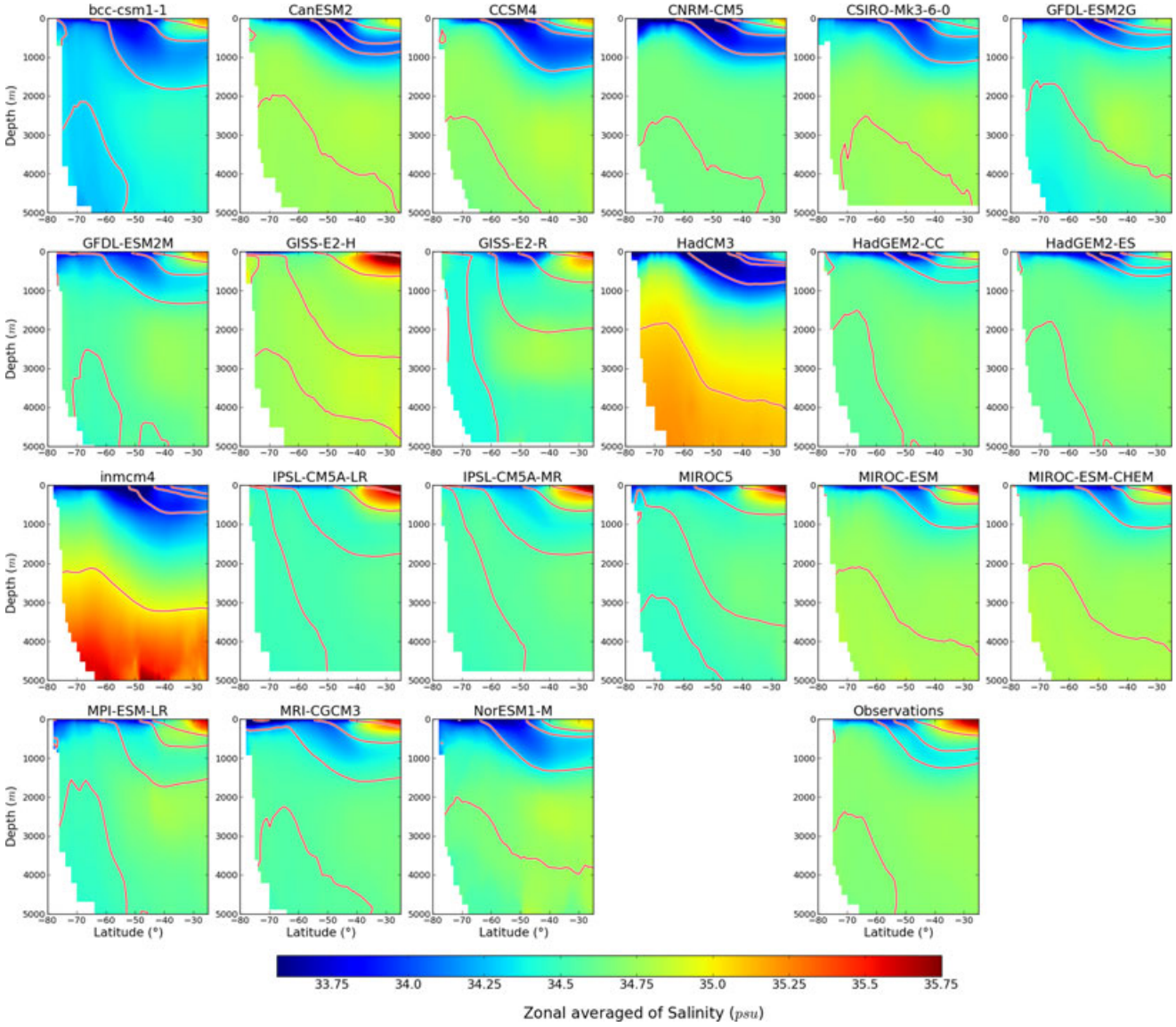

Figure 3. Historical zonal mean salinity for the 21 models. Observations (lower right panel) taken from CARS09. The four red lines mark the boundaries between water masses, and in order of shallowest to deepest are: (a) subtropical water/mode water; (b) mode water/intermediate water; (c) intermediate water/circumpolar deep water; (d) circumpolar deep water/bottom water.

to large warm biases, this model also exhibits a significant fresh salinity bias. Other models compensate warm biases with salty biases (e.g., *GISS-E2-H*, *IPSL-CM5A-LR*; Figure 4a).

[27] The simulated volume of subtropical water is also strongly and consistently biased across models. All models show a smaller volume than that observed by as much as 1.2×10^{16} m^3 (85% of the observed value; Figure 5a; Table 2).

[28] The volume of subtropical water and its area of outcrop are strongly correlated (correlation of 0.76; Figure 5a), reflecting that this water mass is consistently and correctly subducted around the circumpolar belt.

3.2. Mode Water

[29] Subduction into the southern hemisphere subtropical gyres is dominated volumetrically by mode water. Mode water therefore has an important role in climate as it ventilates the Southern Ocean and sequesters heat and carbon. However, we find that mode water is generally poorly represented in the CMIP5 climate models [see also *Downes et al.*, 2010 for an analysis of CMIP3 models]. Figure 2 shows the minimum PV parcels characteristic of mode water along the circumpolar belt at 30° S. All models produce low PV parcels at too light densities and in very different places in the water column compared with the real ocean. This clearly highlights an important shortcoming in the mode water formation process in current-generation climate models. Only one model, *MPI-ESM-LR* shows what might be deemed a realistic mode water layer (Figure 2). Mode waters form and acquire their characteristics in the deep mixed-layers that develop in winter on the northern edge of the Antarctic Circumpolar Current [*Talley*, 1999; *Sallée et al.*, 2006; 2008]. They are then exported across the

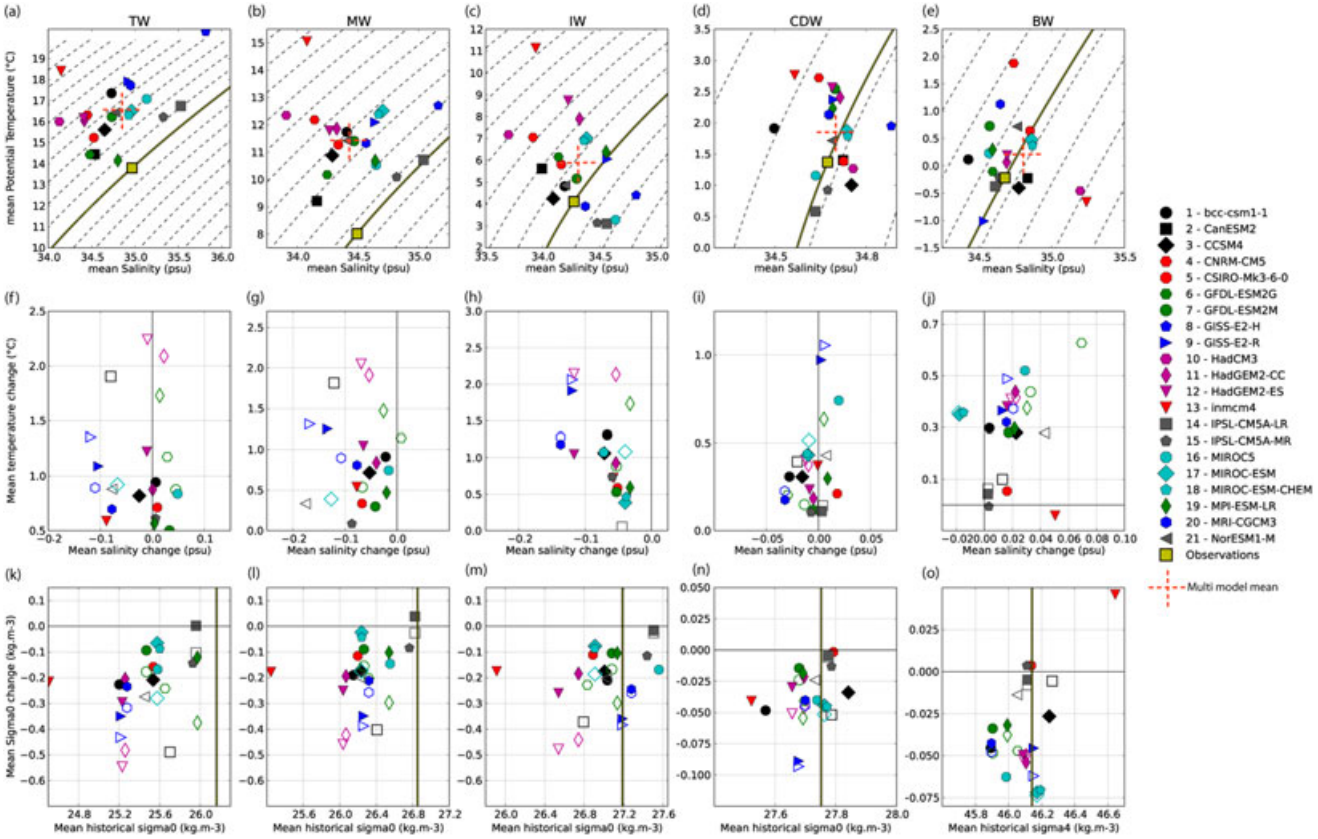

Figure 4. Southern Ocean Temperature-Salinity characteristics and future changes. The upper row, panels (a–e), shows the mean temperature–salinity of each water masses for the period 1970–2000 with superimposed 0.2 kg m^{-3} density contours. The middle row, panels (f–j), shows the mean end of century change in the temperature and salinity characteristic (2070–2100 minus 1970–2000). The bottom row, panels (k–o), shows the mean end of century change in potential density (2070–2100 minus 1970–2000) versus the 1970–2000 mean potential density. The filled symbols represent changes associated with scenario RCP45, and the unfilled symbols represent changes associated with scenario RCP85. Each column is associated with one water mass: from left to right, subtropical water (TW), mode water (MW), intermediate water (IW), circumpolar deep water (CDW) and bottom water (BW). Potential density is referenced to the surface except when associated to bottom water where it is referenced to 4000 m consistent with their very deep storage in the water column.

base of the mixed layer through subduction [*Talley*, 1999; *Sallée et al.*, 2010]. *Sallée et al.*, [2012] found that the CMIP5 models have a consistent bias in their formation of deep mixed-layers, with too deep mixed-layers and too vigorous seasonal cycles in the subtropical regions of the western Indian and Pacific basins. Consistent with this, we find here that most models subduct mode water at too light densities (i.e., subtropical densities) in the western part of the basins, which increases in density very quickly as it shifts into the eastern part of the basins (Figure 2). In contrast to observations where subantarctic mode water dominates the low PV region, models tend to favor the formation of subtropical mode water, which penetrates to shallower depths and lighter densities [see also *Sloyan and Kamenkovich*, 2007 for an analysis of CMIP3 models]. Interestingly, while the mixed layer in the *MPI-ESM-LR* model does not have a realistic spatial pattern, the model's mean mixed layer depth and stratification stand out as the most realistic of the models (Sallée, J. B., E. Shuckburgh, N. Bruneau, A. J. S. Meijers, Z. Wang, and T. J. Bracegirdle, Assessment of the Southern Ocean mixed-layer depth in CMIP5 models: historical bias and forcing response, J. Geophys. Res., in press, 2013.), and in agreement with this, it is found to have the most realistic mode water layer as shown in Figure 2.

[30] Similar to the findings for subtropical water, the light bias in the density of mode water is explained by a warm bias, increased in some models by an associated fresh bias, and counterbalanced in other models by a salty bias (Figure 4b). The similarity is not surprising given that some of the biases must be transferred into deeper layers through diapycnal mixing and that the biases undoubtedly arise from unrealistic air-sea surface flux inputs at the surface subducted down into the mode water layer [*Frölicher et al.*, manuscript in prep.]. The multi-model mean in salinity is in close agreement with observation (∼34.5 psu), despite a large inter-model spread. The multi-model mean temperature shows a warm bias of 3.5°C in the mode water layer (Table 2).

[31] Subduction of mode waters is strongly controlled by Ekman pumping over their outcrop area. Consistent with

Table 2. Mean Water Mass Characteristics[a]

TW	Observation	Historical	RCP4.5 Change	RCP8.5 Change
T (°C)	13.8	16.461	–0.605	01.279
S	34.966	34.779	–0.033	–0.042
σ_0 (kg m^{-3})	26.163	25.44	–0.172	–0.338
Volume (10^{16} m^3)	1.349	0.575	–0.136	0.124
Outcrop (10^{13} m^2)	5.556	3.632	–0.497	00.673
MW				
T (°C)	8.02	11.542	–0.407	0.991
S	34.493	34.472	–0.078	–0.104
σ_0 (kg m^{-3})	26.853	26.235	–0.141	–0.272
Volume (10^{16} m^3)	3.235	1.95	–0.224	0.086
Outcrop (10^{13} m^2)	1.944	02.636	–0.11	–0.266
IW				
T (°C)	4.114	5.851	–0.828	1.387
S	34.275	34.283	–0.067	–0.104
σ_0 (kg m^{-3})	27.189	26.963	–0.16	–0.277
Volume (10^{16} m^3)	3.945	7.426	–2.352	–1.776
Outcrop (10^{13} m^2)	1.556	3.228	–0.488	–0.506
CDW				
T (°C)	1.371	1.849	–0.334	0.412
S	34.673	34.69	–0.005	–0.009
σ_0 (kg m^{-3})	27.752	27.724	–0.032	–0.044
Volume (10^{16} m^3)	32.754	25.235	–1.996	–1.809
Outcrop (10^{13} m^2)	1.993	1.486	–0.127	–0.161
AABW				
T (°C)	–0.22	0.183	–0.262	–0.356
S	34.679	34.742	–0.013	–0.023
σ_4 (kg m^{-3})	46.142	46.124	–0.032	–0.041
Volume (10^{16} m^3)	5.508	7.631	–0.144	–0.213
Outcrop (10^{13} m^2)	0.003	0.057	–0.023	–0.059

[a]Each table list the mean characteristics (temperature, salinity, and density) and volume and outcrop of water masses for: the observation-based climatology, the multi-model mean of historical runs (1976–2005), and the multi-mean change at the end of the 21st century under RCP4.5 and RCP8.5 emission scenarios. From top to bottom, tables correspond to subtropical water (TW), mode water (MW), intermediate water (IW), circumpolar deep water (CDW) and bottom water (BW).

this, we find that the simulated outcrop area and volume of mode water are highly correlated (r = 0.84; Figure 5b). The observed volume and outcrop area of the mode water layer is, however, an outlier from this relationship: it has a large volume, yet a much smaller outcrop area than that simulated by the models. It is likely that models subduct water correctly through Ekman pumping across the outcrop area (hence the good correlation between outcrop and volume), but underestimate the large volumes of water known to subduct through the sloping base of the mixed layer [a process known as lateral induction; e.g., *Huang*, 1991; *Sallée et al.*, 2010]. This latter process must be limited in the models, since they tend to be too stratified and have mixed layers that are too shallow [*Sallée et al.,* 2013].

3.3. Intermediate Water

[32] Intermediate water is often thought of as a denser type of mode water [*Talley et al.*, 1999; *Sallée et al.*, 2010]. Similar to mode water, its characteristics are established in the deep mixed-layers that develop on the northern edge of the Antarctic Circumpolar Current in winter. The intermediate water is then subducted into the interior to ventilate the world's ocean thermocline [*Talley et al.*, 1999]. The subduction occurs in a relatively narrow region directly west of and within the Drake Passage [$\sim$ 290°E; *Talley et al.*, 1999; *Sallée et al.*, 2010]. Consistent with this, we showed in a companion paper that the characteristics and volume of intermediate water are strongly tied to the depth and characteristics of the deep mixed-layers in the southeastern Pacific basin (Sallée, J. B., E. Shuckburgh, N. Bruneau, A. J. S. Meijers, Z. Wang, and T. J. Bracegirdle, in press, 2013).

[33] While some models subduct intermediate waters in regions of the water column that are clearly too stratified (e.g., *CNRM-CM5*; *GFDL-ESM2G*; *HadCM3*; *HadGEM2-CC*; *HadGEM2-ES*; *inmcm4*; see red circles in too high PV in Figure 2), most models do produce a realistic intermediate water layer that fills the entire circumpolar belt. A zonal-mean plot of salinity clearly highlights the minimum salinity layer associated with intermediate water (Figure 3). Because some models have a weaker salinity gradient over their water column, the salinity-minimum tongue is less obvious (e.g., *GISS-E2-H*, *IPSL-CM5A-LR*, *MIROC5*). However, we find overall that the intermediate water layer is much better represented in the CMIP5 climate models than the mode water layer. We believe that this is explained by the subduction process associated with intermediate water. This is mostly linked to the rapid mixed-layer re-stratification when the Antarctic Circumpolar Current flows through Drake Passage [*Sallée et al.*, 2010], which is relatively well simulated in the models analyzed here (Sallée, J. B., E. Shuckburgh, N. Bruneau, A. J. S. Meijers, Z. Wang, and

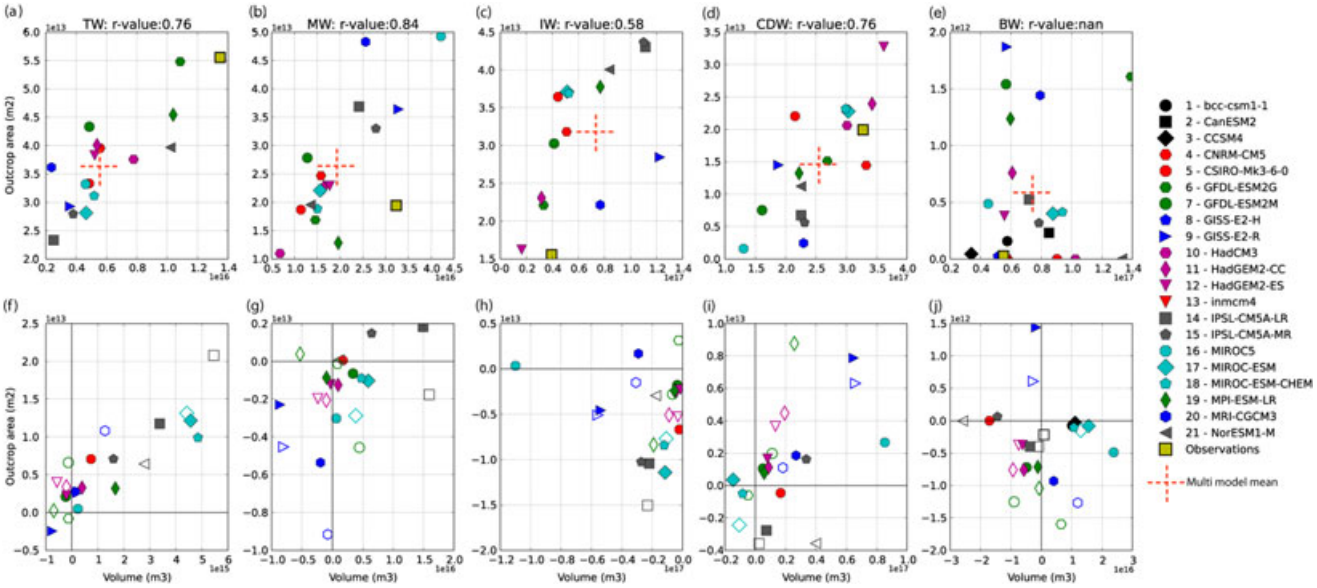

Figure 5. Historical and future changes in Southern Ocean water mass volumes and outcrop areas. The upper row, panels (a–e), shows the mean outcrop area versus volume of each water masses for the period 1970–2000. The bottom row, panels (f–j), shows the mean end of century change in outcrop area versus volume change. The filled symbols represent changes associated with scenario RCP45 and the unfilled symbols represent changes associated with scenario RCP85. Each column is associated with one water mass: from left to right, subtropical water (TW), mode water (MW), intermediate water (IW), circumpolar deep water (CDW) and bottom water (BW).

T. J. Bracegirdle, in press, 2013). Nevertheless, the characteristics of intermediate water vary widely across models. Similar to the findings for subtropical and mode water, we find a large warm bias that offsets the density of intermediate water by up to 0.8 kg m^{-3} (Figure 4c; *inmcm4* has a bias of 1.3 kg m^{-3}, but is a clear outlier). Five models show a slight cold-and-salty density bias toward higher values (*IPSL-CM5A-LR*, *IPSL-CM5A-MR*, *MIROC5*, *MRI-CGCM3*, *GISS-E2-H*). Compared with observations, the multi-model mean density shows a bias of 0.2 kg m^{-3} that mostly arises from a multi-model temperature bias of 1.8°C (Table 2).

[34] In addition to the importance of mixed-layer depth in the southeastern Pacific, which we highlight in a companion paper (Sallée, J. B., E. Shuckburgh, N. Bruneau, A. J. S. Meijers, Z. Wang, and T. J. Bracegirdle, in press, 2013), the outcrop area of intermediate water appears to be an important component for setting the subducted volume (Figure 5c).

3.4. Circumpolar Deep Water

[35] Circumpolar deep waters are formed by deep convection in the North Atlantic basins, and flow southward into the Southern Ocean. They then upwell to the ocean surface on the Southern side of the Antarctic Circumpolar Current and play a key role both in the natural carbon cycle [e.g., *Le Quére et al.*, 2009], and in sea-ice and Antarctic continental shelf processes [e.g., *Thoma et al.*, 2008].

[36] The volume of circumpolar deep water is generally less than that observed (multi-model mean volume of 25.2×10^{16} m^3 for an observed value of 32.7×10^{16} m^3; Figure 5d and Table 2). However, *HadGEM2-ES* and *HadGEM2-CC* have slightly larger volumes of circumpolar deep water that appear to be associated with particularly thin mode and intermediate water layers (Figures 3 and 5d). Given that mode, intermediate and circumpolar deep waters are crucial for the sequestration of natural carbon dioxide through the biological pump and the uptake of anthropogenic carbon dioxide in the Southern Ocean, we expect that the biases in these two models would have a significant impact on their simulated carbon cycles.

[37] In contrast to the lighter water masses described above, circumpolar deep waters have a much smaller bias in temperature and density (multi-model mean temperature of 1.8°C compared with an observed value of 1.4°C; and multi-model mean density of 27.72 kg m^{-3} for an observed value of 27.75 kg m^{-3}; see Figure 4d and Table 2). This reflects the fact that circumpolar deep waters are not formed in the Southern Ocean where the largest air-sea heat flux excess bias is found [*Frölicher et al.*, manuscript in prep.]. Similar to the findings for lighter water masses, *inmcm4* is found to have the largest temperature bias (Figures 4a–4d), which indicates that it is likely that the warm bias is transferred to the circumpolar deep water layer through vertical mixing from layers lying above. While the bias in temperature is much smaller than in lighter layers, the circumpolar deep water biases (which are up to 1.5°C) can have dramatic implications when the water upwells and comes into contact with sea-ice. *Turner et al.* [2013] found that many CMIP5 models have a tendency to produce much less Antarctic sea-ice than is observed, with significant implications for the global climate due to the albedo effect of sea-ice.

3.5. Antarctic Bottom Waters

[38] The most striking spread in the representation of water masses between the models is found in bottom water.

We acknowledge that our water mass definition may not capture bottom waters perfectly across all models. However, it provides a consistent way of pinpointing key differences. In some models, the bottom water layers rise to the surface (e.g., *IPSL-CM5A-LR*, *IPSL-CM5A-MR*, *GISS-E2-R*; (Figure 3), while in others they are concentrated in a small deep region at high latitudes (e.g., *MIROC5*, *MRI-CGCM3*, *CCSM4*, *bcc-csm1-1*, *HadGEM2-CC*, *HadGEM2-ES*), and in some others a thick layer extends to 30°S (e.g., *inmcm4*, *HadCM3*). This wide variety of bottom water representations is summarized clearly by a plot of outcrop versus volume (Figure 5). The volume of bottom water ranges from 0.3 to 1.4 × 10^{17} m^3 depending on the model. The multi-model average volume is larger than observed by about 20% (7.6 × 10^{16} m^3, compared with an observed value of 5.5 × 10^{16} m^3; see Figure 5e and Table 2). The *GFDL-ESM2G* and *NorESM1-M* models have too large a volume of bottom water (∼14 × 10^{16} m^3), while at the other end of the spectrum, the *CCSM4* model produces only 3 × 10^{16} m^3.

[39] The characteristics of bottom water also vary widely across the models (Figure 4e). The *HadCM3* and *inmcm4* models are strongly biased in salinity (∼35.25 psu, compared with an observed value of 34.6 psu), which in turn biases their density by more than 0.4 kg m^{-3}. In contrast the *bcc-csm1-1* model has a fresh bias of about 0.2 psu, which produces lighter bottom water than observed by about 0.2 kg m^{-3}. Similar light biases are artificially produced by warm bottom water in the *CNRM-CM5*, *MRI-CGCM3* and *GFDL-ESM2M* models. Overall, the multi-model mean density of bottom water is very close to the observed value (within 0.02 kg m^{-3}), which is due to compensation between an overall warm bias (0.4°C) and a salty bias (0.06 psu).

[40] The process of bottom water formation has been described in several previous studies [e.g., *Foster and Carmack* 1976; *Baines and Condie* 1998; *Orsi et al.* 1999] and includes complex shelf processes (incorporating Antarctic sea-ice and ice-shelf processes). Due to the considerable challenge of modeling shelf processes, and despite considerable improvement in the last few years, no climate model to date has been capable of correctly simulating the properties of the abyssal oceans. Climate models use a variety of different parameterizations to form and convect bottom water, which do not translate into an outcrop/volume relationship. Issues involved with bottom water biases in models are tightly linked with their parameterization, and an analysis of this is beyond the scope of the present paper. We therefore leave the questions concerning biases in the volume and outcrop of bottom water for a future study.

4. Future Changes of Water Mass Characteristics Under Increased Radiative Forcing

[41] The most consistent future change simulated across all models and all water masses under increased radiative forcing is a warming throughout the water-column (Figures 4f–4j). Under RCP8.5, the warming is on average about 30–60% larger than that under RCP4.5 (Table 2). The largest warming is mostly concentrated in subtropical, mode and intermediate water layers, which are subducted from the surface and therefore have an efficient connection with the atmosphere. The multi-model warming for these three water masses is respectively 0.61°C, 0.41°C, and 0.83°C under RCP4.5, and 1.30°C, 0.99°C, and 1.39°C under RCP8.5. In deeper layers, the multi-model mean warming under RCP4.5 is smaller than the lighter waters; 0.33°C for circumpolar deep waters and 0.26°C for bottom water (resp. 0.41°C and 0.36°C under RCP8.5).

[42] Future changes in salinity are less consistent, particularly between water masses (Figures 4f–4j). For subtropical water, the change in salinity depends on the model and, because of the spread, no clear differences between changes under RCP4.5 and RCP8.5 are apparent (Figure 4f and Table 2). The salinity change in the subtropical water layer ranges from –0.10 psu (e.g., *inmcm4* under RCP4.5, *GISS-E2-H* and *GISS-E2-R* under RCP4.5 and RCP8.5) to +0.05 psu (e.g., *MIROC5* under RCP4.5; *GFDL-ESM2M* under RCP8.5). The multi-model mean salinity change are correspondingly very small compared to their large change in temperature (–0.03 psu for RCP4.5 and –0.04 psu for RCP8.5; Table 2). In contrast, mode and intermediate waters have a very consistent freshening under RCP4.5 and RCP8.5 (Figures 4g–4h). This agrees well with the results described in Sallée et al. (2012), where a consistent increase of freshwater flux input in the region of mode and intermediate water formation at the ocean surface was found under both RCP4.5 and RCP8.5. On average, under RCP4.5 models simulate a freshening of 0.08 psu for mode water and 0.07 psu for intermediate water, which both rise to 0.10 psu under RCP8.5 (Table 2).

[43] Salinity changes in the circumpolar deep water layer are much smaller, and most models simulate almost no change or a slight freshening. We speculate that warming and freshening changes in the circumpolar deep water layer penetrate the water column through isopycnal and vertical mixing at the boundary with the ventilated layers. Mixing would be the only process efficient enough to propagate the signal deep enough in this non-ventilated layer within the 100 year model runs, since circumpolar deep water circulation is associated with time-scale of 500–1000 years to be transported from its formation region in the North Atlantic to the Southern Ocean [e.g., *DeVries and Primeau*, 2011].

[44] In contrast with recently observed decadal trends [e.g., *Rintoul*, 2007] , bottom waters over the 21st century are projected in most of the models to become saltier (Figure 4j). While beyond the scope of the present study, more work on the response of Antarctic sea-ice is needed to fully understand the increased salinity in the simulated bottom water. We can only speculate here that this change would be consistent with a change in the seasonality of sea-ice extent: a larger reduction of sea-ice in summer than in winter (e.g., due to albedo feedback) would result in larger sea-ice formation and salt rejection in fall/winter seasons, when bottom water forms. We note, however, that the only two models that predict a freshening of bottom water (*MIROC-ESM* and *MIROC-ESM-CHEM*) are isopycnal models and therefore probably better simulate shelf overflows of bottom water.

[45] Future changes in temperature and salinity characteristics translate into an overall lightening of the water column (Figures 4k–4o and Table 2) that is larger at the surface and in ventilated layers (0.2–0.4 kg m^{-3}) than in deep layers (0.03–0.04 kg m^{-3}). Under RCP4.5, the multi-model mean reduction in density is 0.14–0.17 kg m^{-3}

(or 0.27–0.34 kg m^{-3} under RCP8.5) for subtropical, mode, and intermediate waters, and 0.03–0.04 kg m^{-3} (or 0.04–0.05 kg m^{-3} under RCP8.5) for circumpolar deep water and bottom water (Table 2). Although there are some hints of state dependency between the historical and future ocean states (Figures 4k–4o; the larger the historical bias, the larger the future change), these dependencies have correlations of less than 0.4), so, we conclude that we do not find any clear state dependency.

[46] We show in a companion paper that all CMIP5 models simulate an overall reduction of the volume of the ventilated layer (the sum of mode and intermediate water volumes) under RCP4.5 and RCP8.5, associated with a shallowing of the mixed-layer in their formation regions (Sallée, J. B., E. Shuckburgh, N. Bruneau, A. J. S. Meijers, Z. Wang, and T. J. Bracegirdle, in press, 2013). However, as mentioned above, the volume of water masses is also tightly linked to their corresponding outcrop area in the Southern Ocean. The CMIP5 models tend to predict an increase of subtropical water outcrop and volume in the future under RCP4.5 and RCP8.5, concomitant with a contraction of the outcrop and volume of the subducted mode and intermediate water (Figure 5f–5h). We find a reduction of 30% in the volume and 15% in the outcrop area for intermediate waters (Table 2). There is a large inter-model spread about these means and as a result no significant differences between RCP4.5 and RCP8.5 are detected. Future changes in outcrop surface area would significantly influence carbon and heat uptake [*Russell et al.*, 2006; *Séférian et al.*, 2012]. For instance, *Séférian et al.* [2012] found, by analyzing the IPSL model, that outcrop surface area change is the dominant fingerprint of climate change on the net cumulative carbon uptake of the Southern Ocean. Interestingly, and consistent with previous studies that have focused on a single model analysis, we find a clear and significant multi-model correlation between atmospheric jet shift and changes in outcrop area of subtropical and intermediate water [*Russell et al.*, 2006; *Séférian et al.*, 2012]. A southward shift of the westerlies is associated with an expansion of the subtropical water outcrop, and a contraction of the intermediate water outcrop (Figure 6). Consistent with these changes, almost all CMIP5 models simulate a southward shift of the subtropical gyres, displacing the ACC northern boundary polewards [*Meijers et al.*, 2012].

[47] These changes are also associated with a significant expansion of the outcrop and volume of circumpolar deep water (multi-model mean increase of ∼10% for both volume and outcrop; Table 2). In contrast, bottom water undergoes a significant reduction of its outcrop region, but this does not appear to be particularly linked to a consistent volume change (Figure 5j).

5. Southern Ocean Water Mass Circulation

[48] As discussed above, Southern Ocean water masses circulate in a two-cell system that is illustrated schematically in Figure 1. In contrast to the ACC transport, the strength of this circulation can only be estimated by an indirect method such as via inverse models. A number of studies have inverted the observed structure of the Southern Ocean water column to estimate the intensity of this overturning circulation [e.g., *Talley*, 2003; *Talley et al.*, 2003; *Talley*, 2008; *Sloyan and Rintoul*, 2001; *Lumpkin and Speer*, 2007]. Two main groups of methods have been applied (geostrophic velocity with empirical reference levels, and box inverse methods), but significant uncertainties still remain in the estimate of the strength of the circulation as a result of the sensitivity of these methods to empirical choices. Nevertheless, a consistent picture stands out with a southward flow of subtropical water at the surface of 5–10 Sv, a northward export of mode water and intermediate water of 8–12 Sv, a southward flux of circumpolar deep water into the Southern Ocean of 20–50 Sv, and a northward export of bottom water of 25–45 Sv (Figure 1, blue bars). Despite the large uncertainties, these studies provide an overall structure and envelope against which to evaluate climate models.

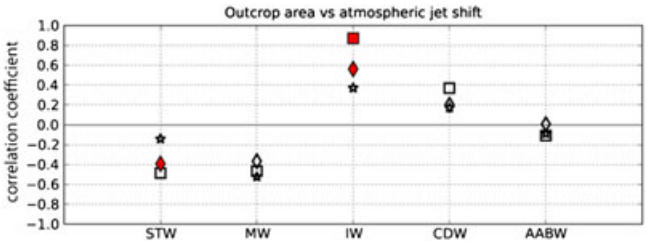

Figure 6. Across model-correlation between the end of 21st century change in the latitude of the atmospheric jet and the outcrop are of each water mass: (star marker) RCP 8.5 scenario only, (square marker) RCP4.5 scenario only, (diamond marker) RCP4.5 and RCP8.5 scenarios. Red markers indicate that the correlation is significant above the 95% confidence limit. A positive (negative) correlation denotes that the southward shift of the jets is associated to an increase (decrease) of the outcrop area.

[49] Interestingly, models are relatively consistent in their simulation of transport at 30°S (see Figures 1 and 7b, black bars). Overall, the modeled upper cell is slightly more intense than observed—although within the observational error envelope (14 ± 7 Sv for mode water and intermediate water export)—and the bottom cell is much weaker than that observed (11 ± 5 Sv of bottom water export). We note that there are two outliers that have much weaker overturning cells: *MIROC5* and *MPI-ESM-LR* (Figure 7b, black bars). Unfortunately, the observation-based studies of how this circulation is closed within the Southern Ocean are rather limited due to both the complexity of the processes involved and sparse observations. In models, however, we can infer the volume transformed at the surface or by interior processes via the amount of water entering and leaving the Southern Ocean (see section 2; results presented in Figure 7). Consistent with *Sallée et al.* [2010], modeled mode water is mostly formed from an equatorward inflow of intermediate water in the surface layer. Then, mode water is formed and subducted due to a net buoyancy loss driven by cooling and evaporation. Consistent with *Downes et al.* [2011], who analyzed the three GFDL models and ocean reanalysis, we find that simulated intermediate water is mostly formed through interior processes and destroyed at the surface through warming. Note that the relatively high interior transformation rates include diapycnal mixing in the mixed layer. Although we cannot untangle mixed-layer processes from interior mixing, it is worth mentioning that

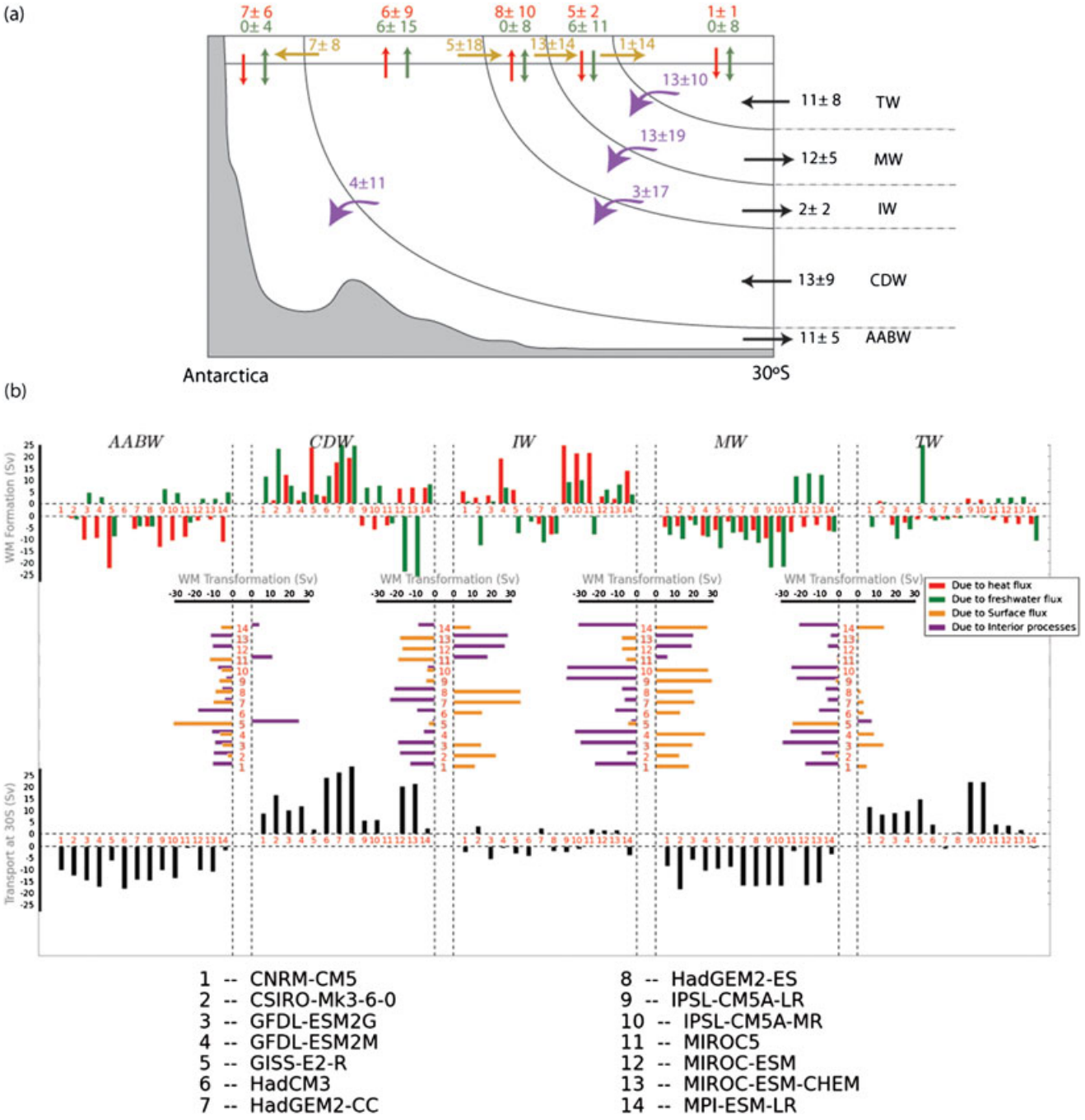

Figure 7. Water mass formation, transformation and export out of the Southern Ocean. (a) Schematic showing the multi-model mean formation, transformation and transport of water masses at 30°S: formation from heat flux (red) and freshwater flux (green); transformation from surface buoyancy flux (yellow) and interior processes (purple); export across the 30°S boundary (black). All numbers are in Sv. (b) Same as top panel, but expanded for each individual models. Colors correspond to top panel colors.

Sallée et al. [2006, 2008] estimated substantial diapycnal mixing within the mixed layers in the mode and intermediate water density classes from observations. Circumpolar deep water that enters the Southern Ocean at 30°S in the models is mostly destroyed at the surface by net buoyancy gain due to both warming and freshening. The upwelled circumpolar deep water in the models is then converted into intermediate water and denser bottom water, which sinks into the interior due to cooling.

[50] It is important to clarify here that while intermediate water is not formed at the surface in the circumpolar average, this water mass is still ventilated, as indicated earlier in this paper. Indeed, the circumpolar average hides very localized subduction spots, mostly in the east Pacific and through Drake Passage [*Sallée et al.*, 2010], which create a very large input of ventilated water into the layer. In agreement with observations, the multi-model mean structure clearly shows a large reduction in PV in the inter-

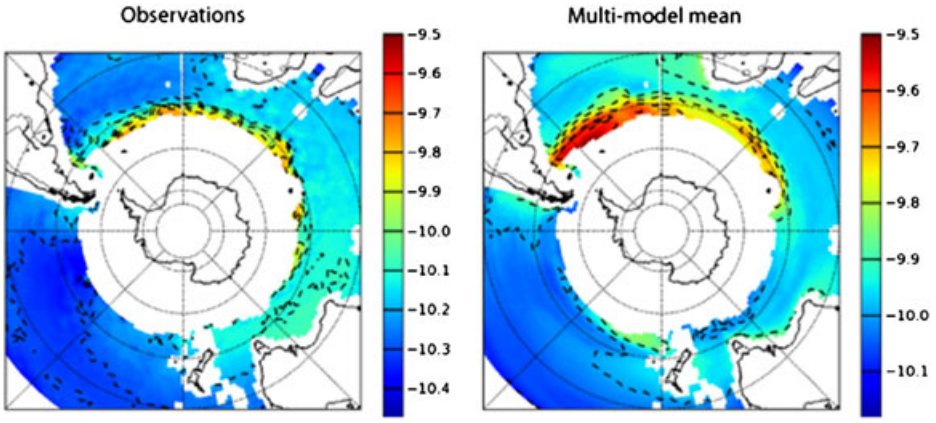

Figure 8. Potential vorticity (PV) in the intermediate water mass layer ($\log_{10}$ of PV is shown, m^{-1} s^{-1}). (left) Observed mean and (right) multi-model mean.

mediate water layer, which originates from the east Pacific region (Figure 8). Low PV water indicates young, recently ventilated water. The low PV tongue then spreads into the subtropical gyres. Nevertheless, beyond the circumpolar structure, the averaged upwelling found in the intermediate water density class would suggest that the ventilated water is reabsorbed in other regions along the circumpolar belt. We find that all of the 8 Sv of upwelled intermediate water at the surface is transferred into the mode water density class (yellow arrow in Figure 7), which then sinks into the interior and is transformed back into intermediate water. Therefore, the intermediate water layer does indeed consist of recently ventilated water.

[51] Changes in the circulation over the 21st century under increased radiative forcing scenarios are strongest at the surface, with increased northward surface circulation consistent with increased westerly wind intensity [*Bracegirdle et al.*, 2013; Figure 9]. The increased northward export peaks directly south of the intermediate water density class, creating a convergence in the intermediate water density class, which results in increased intermediate water subduction. Most of the increased subducted water is, however, redistributed within the Southern Ocean interior by interior mixing processes. As a result, changes in transport at 30°S are negligible, while the imprinted changes at the surface would have suggested an increase in the upper cell of the Southern Ocean overturning (Figure 9). The most significant change in transport at 30°S are a slight decrease of bottom water export, which is mostly balanced by a decreased southward transport of subtropical water.

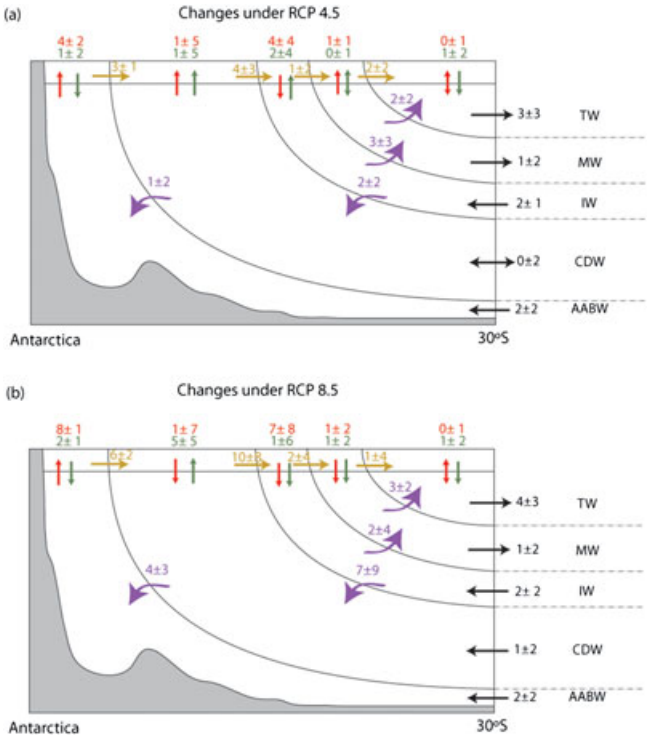

Figure 9. Future changes in water mass formation, transformation and export out of the Southern Ocean under (a) RCP4.5 and (b) RCP8.5. Details are the same as in Figure 7a caption.

6. Conclusions and Discussion

[52] The representation of the Southern Ocean water mass properties and circulation has been evaluated in 21 climate models from the CMIP5 ensemble. To facilitate this comparison, we designed an objective, auto-adaptive approach that isolates Southern Ocean water masses based solely on the two most widely available hydrological properties: temperature and salinity. A key strength of this approach is that it can be applied consistently to compare both observations and models, which tend to have very different properties and circulation characteristics. Here, for each Southern Ocean water mass, we used the approach to examine the mean climatological representation of water mass volume, temperature, salinity, circulation, transformation and outcrop area, and how these properties change under future climate forcing scenarios.

[53] On average, the water masses of the Southern Ocean in the CMIP5 models are too warm and light over the entire water-column. The largest biases are found in the ventilated layers, indicating that most of the bias must be related to excess heat uptake at the ocean surface [*Frölicher et al.*: manuscript in prep.] and exported in the interior through

subduction. Warm biases are also present in the deeper layers, but they are smaller. Under increased radiative forcing, all simulated water masses warm significantly, with the largest warming occurring in the ventilated layer. This again highlights the efficient climate signal propagation from the atmosphere to the ocean interior in these layers. Mode and intermediate waters also tend to freshen, consistent with an increased freshwater input in their formation region [*Sallée et al*, 2012]. Yet, in contrast to observations [e.g., *Rintoul*, 2007], bottom water is simulated to become slightly saltier.

[54] There is a large spread in the representation of bottom water across models and the general representations of density structures south of the ACC. In turn, this spread is associated to significant inter-model variations in the representation of the subpolar gyres, which itself is associated to biases in the position of the ACC southern boundary, and is the single strongest control on the net ACC transport [*Meijers et al.*, 2012].

[55] Under increased radiative forcing, water masses are simulated to undergo significant changes in outcrop area and volume. The largest volume changes occur in the intermediate and circumpolar deep water layers, with a reduction of intermediate water that is mostly redistributed into circumpolar deep water. Consistent with previous studies, the poleward shift of the atmospheric jet is associated with an expansion of the subtropical water outcrop, and a reduction of the outcrop of intermediate water in the models as the northern boundary of the ACC is forced polewards [*Meijers et al.*, 2012]. *Bracegirdle et al.* [2013] showed that the shift in the atmospheric jet is characterized by two main phases: one period with little change (2000–2049) that is associated with a rapid recovery of stratospheric ozone, and a second period (2050–2100) with a shift that is strongly dependent on the amount of radiative forcing. The results presented here suggest that we might expect similar behavior for the outcrop area change. Intermediate waters are of key importance to the sequestration and transport of heat, salt, nutrient and gases such as carbon dioxide [e.g., *Sallée et al.*, 2012] and, therefore, their outcrop area is crucial for determining the net cumulative carbon uptake of the Southern Ocean [e.g., *Séférian et al.*, 2012].

[56] We have found that the CMIP5 climate models on average have a slightly more intense upper cell and weaker bottom cell than observation-based reconstructions. Consistent with *Downes et al.* [2011], who analyzed previous versions of the GFDL climate models, intermediate water is mostly formed from mode water by interior processes in the models, and destroyed at the surface, while mode waters are formed at the surface. Under increased radiative forcing, the surface transformation of water suggests an intensification of the upper cell circulation, with increased upwelling of circumpolar deep water and increased subduction of intermediate water. These changes are balanced by interior processes, which transform intermediate water back into circumpolar deep water in approximately equal quantities. We note that interior processes include mixed-layer processes in this framework, so the circulation might compensate either in the interior ocean or within the mixed-layer, diminishing the circulation changes. An increased meridional density gradient across the ACC, which is found in all models under increased radiative forcing [*Meijers et al.*, 2012], would be expected to give rise to more intense lateral mixing in the mixed-layer and more intense interior mixing.

[57] Many of the biases and future changes identified in this study are expected to have significant impacts on the marine carbon cycle. The marine carbon cycle is strongly driven by the combination of changes in local water mass properties, outcrop area, water mass volume and the large scale overturning circulation [e.g., *Le Quére et al.*, 2009; *Séférian et al.*, 2012]. While beyond the scope of this study the detailed changes of overturning within the Southern Ocean and their implications for the carbon cycle will need to be investigated in a future study.

[58] **Acknowledgments.** This study is part of the British Antarctic Survey Polar Science for Planet Earth Programme. It was funded by The UK Natural Environment Research Council (grant reference number NE/J005339/1). We acknowledge the World Climate Research Programme's Working Group on Coupled Modeling, which is responsible for CMIP, and we thank the climate modeling groups (listed in Table 1 of this paper) for producing and making available their model output. For CMIP the U.S. Department of Energy's Program for Climate Model Diagnosis and Intercomparison provides coordinating support and led the development of software infrastructure in partnership with the Global Organization for Earth System Science Portals. Z.W. is supported by China National Natural Science Foundation (NSFC) Project (41276200), the Special Program for China Meteorology Trade (Grant No. GYHY201306020), the Chinese National Key Basic Research Program (2010CB950301), and by a project funded by the Priority Academic Program Development of Jiangsu Higher Education Institutions (PAPD). T.R. is supported through EU FP7 project CARBOCHANGE "Changes in carbon uptake and emissions by oceans in a changing climate", which received funding from the European Commission's Seventh Framework Programme under grant agreement no. 264879. Finally, we thank the British Atmospheric Data Centre for downloading and managing the model output data and making them available to us.

References

Baines, P. G., and S. Condie (1998), Observations and modelling of Antarctic downslope flows: A review, *Ocean, Ice and Atmos.: Interac. at the Antarct. Cont. Marg.*, *75*, 29–49.

Bindoff, N. L., and T. J. McDougall (2000), Decadal changes along an Indian Ocean Section at 32 S and their interpretation, *J. Phys. Ocean.*, *30*, 1207–1222.

Bracegirdle, T. J., E. Shuckburgh, J. B. Sallée, Z. Wang, A. J. S. Meijers, N. Bruneau, and L. J. Wilcox (2013), Assessment of surface winds over the Atlantic, Indian and Pacific Ocean sectors of the Southern Hemisphere in CMIP5 models: historical bias, forcing response, and state dependency, *J. Geophys. Res. Atmos.*, *118*, 547–562, doi:10.1002/jgrd.50153.

GER Deacon (1937), The hydrology of the Southern Ocean, *Discov. Rep.*, *XV*, 1–124.

DeVries, T., and F. Primeau (2011), Dynamically and observationally constrained estimates of water-mass distributions and ages in the Global Ocean, *J. Phys. Ocean.*, *41*, 2381–2401, doi:10.1175/JPO-D-10-05011.1.

Downes, S. M., N. L. Bindoff, and S. R. Rintoul (2010), Changes in the subduction of Southern Ocean water masses at the end of the 21st century in eight IPCC models, *J. Climate*, *23*, 6526–6541, doi: 10.1175/2010JCLI3620.1.

Downes, S. M., N. L. Bindoff, and S. R. Rintoul (2009), Impact of climate change on the subduction of mode and intermediate water masses in the Southern Ocean, *J. Climate*, *22*, 3289–3302, doi: 10.1175/2008JCLI2453.1.

Downes, S. M., A. Gnanadesikan, S. M. Griffies, and J. L. Sarmiento (2011), Water Mass Exchange in the Southern Ocean in Coupled Climate Models, *J. Phys. Ocean.*, *41*, 1756–1771

Foster, T. D., and E. C. Carmack (1976), Frontal zone mixing and Antarctic Bottom water formation in the southern Weddell Sea, *Deep-Sea Res.*, *23*, 301–317.

Gille, S. T. (2002), Warming of the Southern Ocean since the 1950s, *Science*, *295*, 1275–1277.

Gnanadesikan, A., J. P. Dunne, R. M. Key, K. Matsumoto, J. L. Sarmiento, R. D. Slater, and P. S. Swathi (2004), Oceanic ventilation and biogeochemical cycling: Understanding the physical mechanisms that produce

realistic distributions of tracers and productivity, *Global Biogeochem. Cycles*, *18*(4), GB4010, doi:10.1029/2003G8002097.

Huang, R. X. (1991), The three-dimensional structure of wind-driven gyres: Ventilation and subduction, *Rev. Geophys.*, *29*((Suppl.), National Report to the IUGG, 1987-1990), 590–609.

Iudicone, D., I. Stendardo, O. Aumont, K. B. Rodgers, G. Madec, L. Bopp, O. Mangoni, and M. Ribera d'Alcala (2010), Watermasses as a unifying framework for understanding the Southern Ocean carbon cycle, *Biogeosciences Discuss.*, *7*, 3392–3451, doi:10.5194/bgd-7-3393-2010.

Le Quéré, C., et al. (2009), Trends in the sources and sinks of carbon dioxide, *Nat. Geosci.*, *2*, 831–836, doi:10.1038/NGE0689.

Le Quéré, C., C. Rodenbeck, E. T. Buitenhuis, T. J. Conway, R. Langenfelds, A. Gomez, C. Labuschagne, M. Ramonet, T. Nakazawa, and N. Metzl (2007), Saturation of the Southern Ocean CO2 sink due to recent climate change, *Science*, *316*(5832), 1735–1738, doi:10.1126/science.1136188.

Lumpkin, R., and K. Speer (2007), Global ocean meridional overturning, *J. Phys. Ocean.*, *37*, 2550–2562, doi:10.1175/JPO3130.1.

Marshall, J., D. Jamous, and J. Nilsson (1999), Reconciling thermodynamic and dynamic methods of computation of water-mass transformation rates, *Deep-Sea Res. (1 Oceanogr. Res. Pap.)*, *46*(4), 545–572.

Marshall, J., and K. Speer (2012), Closure of the meridional overturning circulation through Southern Ocean upwelling, *Nat. Geosci.*, *5*(3), 171–180, doi:10.1038/ngeo1391.

McCartney, M. S. (1977), Subantarctic mode water, in *A Voyage of Discovery: George Deacon 70th Anniversary Volume*, edited by Angel, M. V., Supplement to Deep-Sea Research, Pergamon Press, Oxford, 103–119.

Meijers, A. J. S., E. Shuckburgh, N. Bruneau, J. B. Sallée, T. J. Bracegirdle, and Z. Wang (2012), Representation of the Antarctic Circumpolar Current in the CMIP5 climate models and future changes under warming scenarios, *J. Geophys. Res.*, *117*, C12008, doi:10.1029/2012JC008412.

Meinshausen, M., et al. (2011), The RCP greenhouse gas concentrations and their extensions from 1765 to 2300, *Climatic Change*, *109*, 213–241, doi:10.1007/s10584-011-0156-z.

Meredith, M., et al. (2011), Sustained monitoring of the Southern Ocean at Drake Passage: Past achievements and future priorities, *Rev. Geophys.*, *49*, RG4005, doi:10.1029/2010RG000348.

Orsi, A. H., G. C. Johnson, and J. L. Bullister (1999), Circulation, mixing, and production of Antarctic Bottom Water, *Prog. Oceanogr.*, *43*(1), 55–109.

Ridgway, K. R., J. R. Dunn, and J. L. Wilkin (2002), Ocean interpolation by four-dimensional weighted least squares application to the waters around Australasia, *J. Atmos. Ocean. Tech.*, *19*, 1357–1375, doi:10.1175/1520-0426(2002)019<1357:OIBFDW>2.0.CO;2.

Rintoul, S. R. (2007), Rapid freshening of Antarctic Bottom Water formed in the Indian and Pacific oceans, *Geophys. Res. Lett.*, *34*(6), L06606, doi:10.1029/2006GL028550.

Russell, J. L., K. W. Dixon, A. Gnanadesikan, R. J. Stouffer, and J. R. Toggweiler (2006), The Southern Hemisphere westerlies in a warming world: Propping open the door to the deep ocean, *J. Climate*, *19*, 6382–6390, doi:10.1175/JCLI3984.1.

Sallée, J. B., N. Wienders, K. Speer, and R. Morrow (2006), Formation of subantarctic mode water in the southeastern Indian Ocean, *Ocean Dynamics*, *56*(5), 525–542, doi:10.1007/s10236-005-0054-X.

Sallée, J. B., R. Morrow, and K. Speer (2008), Eddy heat diffusion and Subantarctic Mode Water formation, *Geophys. Res. Lett.*, *35*(5), L05607, doi:10.1029/2007GL032827.

Sallée, J. B., R. Matear, S. R. Rintoul, and A. Lenton (2012), Localised subduction of anthropogenic carbon dioxide in the Southern Hemisphere oceans, *Nat. Geosci.*, *5*, 579–584, doi:10.1038/ngeo1523.

Sallée, J. B., K. Speer, S. R. Rintoul, and S. Wijffels (2010), Southern Ocean thermocline ventilation, *J. Phys. Ocean.*, *40*(3), 509–529, doi:10.1175/2009JPO4291.1.

Sallée, J. B., E. Shuckburgh, N. Bruneau, A. J. S. Meijers, Z. Wang, and T. J. Bracegirdle (2013), Assessment of the Southern Ocean mixed-layer depth in CMIP5 models: historical bias and forcing response, *J. Geophys. Res.*, doi:10.1002/jgrc.20157.

Sarmiento, J. L., N. Gruber, M. A. Brzezinski, and J. P. Dunne (2004), High-latitude controls of thermocline nutrients and low latitude biological productivity, *Nature*, *427*, 56–60, doi:10.1038/nature02204.

Séférian, R., D. Iudicone, L. Bopp, T. Roy, and G. Madec (2012), Water mass analysis of effect of climate change on air-sea CO2 fluxes: The Southern Ocean, *J. Climate*, *25*(11), 3894–3908, doi:10.1175/JCLI-D-11-00291.1.

Sloyan, B., and I. V. Kamenkovich (2007), Simulation of subantarctic mode and Antarctic intermediate waters in climate models, *J. Climate*, *20*, 5061–5080, doi:10.1175/JCLI4295.1.

Sloyan, B., and S. R. Rintoul (2001), The Southern Ocean limb of the global deep overturning circulation, *J. Phys. Ocean.*, *31*, 143–172.

Speer, K., S. R. Rintoul, and B. Sloyan (2000), The diabatic Deacon Cell*, *J. Phys. Ocean.*, *30*, 3212–3222.

Speer, K., and E. Tziperman (1992), Rates of water mass formation in the North Atlantic Ocean, *J. Phys. Ocean.*, *22*, 93–104.

Sverdrup, H. U., M. W. Johnson, and R. H. Fleming (1942), *The Oceans: Rheir Physics, Chemistry and General Biology*, Prentice-Hall, EnglewoodCliffs, N. J.

Talley, L. (2003), Shallow, intermediate, and deep overturning components of the global heat budget, *J. Phys. Ocean.*, *33*, 530–560, doi:10.1175/1520-0485(2003)033<0530:SIADOC>2.2CO;2.

Talley, L. (2008), Freshwater transport estimates and the global overturning circulation: Shallow, deep and throughflow components, *Prog. Oceanogr.*, *78*, 257–303, doi:10.1016/j.pocean.2008.05.001.

Talley, L. D. (1999), Some aspects of ocean heat transport by the shallow, intermediate and deep overturning circulations, *Geophys. Mono. Ser.*, *112*, 1–22.

Talley, L. D., J. Reid, and P. Robbins (2003), Data-based meridional overturning streamfunctions for the global ocean, *J. Phys. Ocean.*, *16*, 3213–3226, doi:10.1175/1520-0442(2003)016<3213:DMOSFT>2.0.CO;2

Taylor, K. E., R. J. Stouffer, and G. A. Meehl (2012), An overview of CMIP5 and the experiment design, *B AM METEOROL SOC*, *93*, 485–498, doi:10.1175/BAMS-D-11-00094.1.

Thoma, M., A. Jenkins, D. Holland, and S. Jacobs (2008), Modelling circumpolar deep water intrusions on the Amundsen Sea continental shelf, Antarctica, *Geophys. Res. Lett.*, *35*(18), doi:10.1029/2008GL034939.

Turner, J., T. J. Bracegirdle, T. Phillips, G. J. Marshall, and J. S. Hosking (2013), An initial assessment of antarctic sea ice extent in the CMIP5 models, *J Clim.*, doi:10.1175/JCLI-D-12-00068.1

Tziperman, E. (1986), On the role of interior mixing and air-sea fluxes in determining the stratification and circulation of the oceans, *J. Phys. Ocean.*, *16*, 680–693

Walin, G. (1982), On the relation between sea-surface heat flow and thermal circulation in the ocean, *Tellus*, *34*(2), 187–195.